Available online at website: https://journal.bcrec.id/index.php/bcrec

Bulletin of Chemical Reaction Engineering & Catalysis, 19 (3) 2024, 429-441

Research Article

Synthesis of Mesoporous ZnO•SiO_2 Nanocomposite from Rice Husk for Enhanced Degradation of Organic Substances Including Janus Green B under Visible Light

Thu Huong Nguyen[1], Tuan Cuong Vu[2], Trung Phong Le[2], Thu Huyen Nguyen[2], Xuan Truong Do[1], Anh-Tuan Vu[1,*]

[1]School of Chemistry and Life Sciences, Hanoi University of Science and Technology, Hanoi, Viet Nam
[2]Nguyen Gia Thieu High School, Hanoi, Vietnam.

Received: 25th June 2024; Revised: 5th August 2024; Accepted: 5th August 2024
Available online: 8th September 2024; Published regularly: October 2024

Abstract

Rice husk (RH) is often mentioned as an agricultural by-product, often used in the pass as fertilizer and for raw burning. With modern science, RH have been researched and found many new potential benefits and applications. In this study, RH were used to synthesize amorphous SiO_2, which was used to prepare the ZnO•SiO_2 nanocomposites by a hydrothermal method. The as-synthesized materials were characterized by X-ray diffraction (XRD), scanning electron microscopy (SEM), Fourier transform infrared spectroscopy (FT-IR), and N_2 adsorption/desorption isotherm. Their photocatalytic properties were studied by an ultraviolet-vis spectrophotometer and a fluorescence spectrophotometer. The ZnO•SiO_2 nanocomposite has an excellent ability to degrade organic substances such as dyes, antibiotics, caffeine, etc. The effects of operating parameters on the photo-degradation reaction progress, including catalyst dosage, initial dye concentration, and pH of the initial dye were investigated in detail. In addition, the photodegradation rate of the dye on the ZnO•SiO_2 nanocomposite was evaluated using the pseudo-first-order model. The ZnO•SiO_2 nanocomposite can be used as a photocatalyst for wastewater treatment as it detaches much more easily from the solution.

Keywords: Photodegradation; Zinc Oxide; Amorphous Silica; Rice Husk; Janus Green B

How to Cite: T.H. Nguyen, T.C. Vu, T.P. Le, T.H. Nguyen, X.T. Do, A.-T. Vu (2024). Synthesis of Mesoporous ZnO•SiO_2 Nanocomposite from Rice Husk for Enhanced Degradation of Organic Substances Including Janus Green B under Visible Light. *Bulletin of Chemical Reaction Engineering & Catalysis*, 19 (3), 429-441 (doi: 10.9767/bcrec.20175)

Permalink/DOI: https://doi.org/10.9767/bcrec.20175

1. Introduction

Vietnam is a developing country with a large-scale rice sector. Rice husks account for about 20 % by weight of rice seeds and are released into the environment during rice production process. About 11 million tons of rice husks were produced in 2024 [1]. The scientists report that only a small proportion of the rice husks are used as fuel in the milling plants and the surplus of the remaining rice husks has polluted the environment. Rice husk ash (RHA) is obtained after burning the rice husks and consists of about 80% by weight of SiO_2 [2]. The use of rice husks as a source of silica for the production of silica-based materials for applications in industry, chemistry, biology and agriculture is therefore attracting great interest from scientists.

Water pollution is a major problem for aquatic life, public health and environmental quality [3-5]. The disposal of wastewater contaminated with dyes from various industries such as textile, tanning, paper and pulp is a major environmental problem for industry, municipalities and science, as these substances and their degradation products are toxic, carcinogenic and mutagenic to the entire ecosystem [6]. Therefore, industrial wastewater containing dyes must be treated before it is released into the environment. Meanwhile,

* Corresponding Author.
Email: tuan.vuanh@hust.edu.vn (A.-T. Vu)

semiconductor photocatalysis has proven to be one of the most promising methods for wastewater treatment compared to other conventional techniques [7].

Many years ago, SiO_2 was already known as a potential adsorbent for the removal of pollutants in the aquatic environment. In 2016, M.A. Rafiq and colleagues [8] used the electrospinning method to synthesize porous SiO_2 nanofibers that remove toxic dyes in an aqueous environment. The result of this study shows that the maximum adsorption capacity for methyl orange and safranin O was 730.9 and 960.4 mg/g, respectively [8]. In 2019, in an effort to research environmentally friendly materials, Thi Thu Hoang and her colleagues successfully synthesized porous SiO_2 from rice husk which is an agricultural by-product. This porous SiO_2 can remove methyl blue relatively well (91.9 % after 50 min of adsorption) [9]. It can be seen that porous SiO_2 is a good adsorbent that has received much attention from scientists in the field of wastewater treatment. The porous SiO_2 is also considered as a potential carrier due to its excellent adsorption capacity. Recently, many scientists have explored the modification of SiO_2 to obtain materials with superior pollutant treatment capabilities. For example, Anh Tuan Vu and his colleagues [5] fabricated an ethylenediaminetetraacetic acid (EDTA) modified porous silica composite from rice husk in 2024 to improve the removal of Pb^{2+} from aqueous solutions. A large specific surface area and high pore volume of the EDTA-modified porous silica composite (PS-EDTA) were determined to be 496.8 m^2/g and 1.44 cm^3/g, respectively. Under optimal reaction conditions, the PS-EDTA composite showed a Pb^{2+} removal efficiency of 99.98 % and a q_{max} value of 84.70 mg/g [5]. Titanium dioxide–silica materials have been proposed as an alternative to conventional TiO_2 catalysts to facilitate the removal of solids after the photocatalytic reaction. In 2006, José Aguado and colleagues [10] successfully synthesized TiO_2/SiO_2 materials by the sol-gel method. This material has photocatalytic oxidation activity of cyanide in water [10].

ZnO is one of the most important semiconductor photocatalysts due to its high photosensitivity and stability [11]. In 2020, Thi Anh Tuyet Pham and her colleagues [12] synthesized the ZnO nanoparticles via a facile precipitation method. These nanoparticles have excellent photocatalytic ability to degrade 2,2-bis(4-hydroxyphenyl)propane [12]. In 2023, Thu Huong Nguyen and her colleagues [13] studied the tetracycline hydrochloride (TCH) degradation ability of the carnation-like ZnO material. This material showed efficient degradation of TCH with the decomposition efficiency and rate constant of 89.92% and 0.038 min^{-1}, respectively [13]. However, the use of ZnO powder is associated with some difficult problems in terms of performance and recovery. In order to promote the advantages of ZnO and utilize agricultural by-products, the synthesis of $ZnO \cdot SiO_2$ material was explored and used to treat dyes in the water environment. Zn^{2+} was loaded on the surface of porous silica (SiO_2) through the hydrogen bonding between the hydroxyl groups in the hydrothermal process to reduce the primary particle size of zinc oxide (ZnO) and eliminate the agglomeration phenomenon to form a monodisperse state. After calcination of the precursors, dehydration condensation occurred between the hydroxyl groups and the ZnO nanoparticles on porous SiO_2, forming produced the $ZnO \cdot SiO_2$ nanocomposite. The composite produced in this way was used to treat wastewater containing the Janus Green B dye. The properties of the materials were analyzed using modern methods to investigate the influence of morphology and structure on catalytic activity. In addition, the optimal conditions for the photocatalytic degradation of Janus Green B and the stability of the $ZnO \cdot SiO_2$ nanocomposite were also investigated.

2. Materials and Methods

2.1 Materials

Rice husk was collected in Thai Binh province, a region in the Red River Delta in Vietnam. Janus Green B (JGB, 99%) was purchased from Sigma-Aldrich. Zinc nitrate ($Zn(NO_3)_2.6H_2O$, 99%), hexamethylene tetramine ($C_6H_{12}N_4$, 99%), sodium citrate ($C_6H_5NaO_7S.2H_2O$, 99%), sodium hydroxide (NaOH, 99%), cetyl trimetylammonium bromua (CTAB, 99%) were purchased from Merck. Hydrochloric acid (HCl, 36-38%), Tetracycline Hydrochloride (TCH, 99%), Caffeine, Methylence Blue (MB), Congo Red (CR), Tartrazine (TA) were obtained from China. All the chemicals were used without any purification and distilled water was used throughout the experiments.

2.2 Preparation of Porous Silica from Rice Husk

The method for the preparation of porous silica was modified by adding the surfactant CTAB from the previous report [2]. RH was first washed with tap water and rinsed with distilled water in several times to remove the dirt. Then, RH was treated with hydrochloric acid 0.5 M for 30 min at constant stirring to remove metal impurities. Subsequently, it was rinsed with distilled water again to remove excess acid, dried at 100 °C overnight and burned at 600 °C for 2 h under air flow to obtain RHA. An amount of 5 g of RHA was added into 100 mL of NaOH 2 M in an Erlenmeyer flask. The mixture was heated to

about 60 °C for 2 h to completely dissolve the silica in the RHA. The slurry, which consisted of the residue of the digested ash, Na_2SiO_3, water and free NaOH, was then filtered to obtain a Na_2SiO_3 solution with a pH of about 13, as shown in Figure 1(a).

As shown in Figure 1(b), an amount of 2.187 g of CTAB was added to 34 mL of 0.6 N HCl for 6 min. This mixture was added 40 mL of the Na_2SiO_3 solution obtained above, and pH was adjusted to 7.5 - 8.5 with HCl 6 N. After aging this mixture for 24 h at 50 °C, the white gel was obtained and then poured into an autoclave for 48 h at 100 °C. The white solid powder was obtained by filtration and washed with distilled water to remove the excess amounts of surfactant and acid until a neutral pH value. Finally, the white powder was dried at 100 °C and calcined at 600 °C to obtain porous silica.

2.3 Preparation of Porous $ZnO \cdot SiO_2$ Nanocomposite

$ZnO \cdot SiO_2$ nanocomposite was prepared by facile precipitation method [14]. Typically, 0.1 mol of zinc nitrate, 0.1 mol of HMTA and 0.01 mol of sodium citrate were dissolved in a 100 mL beaker. An amount of 0.6001 g of the porous SiO_2 material was added into solution and then sonicated for 20 min. This mixture was heated up to 90 °C for 1 h. The precipitate was filtered and washed serveral times with distilled water. Finally, this powder was dried at 100 °C overnight and calcined at 400 °C for 2 h with a heating rate of 1 °C/min to obtain the $ZnO \cdot SiO_2$ nanocomposite.

2.4 Characterizations

The morphology and size of the as-synthesized materials were observed by a field emission scanning electron microscopy (FE-SEM,

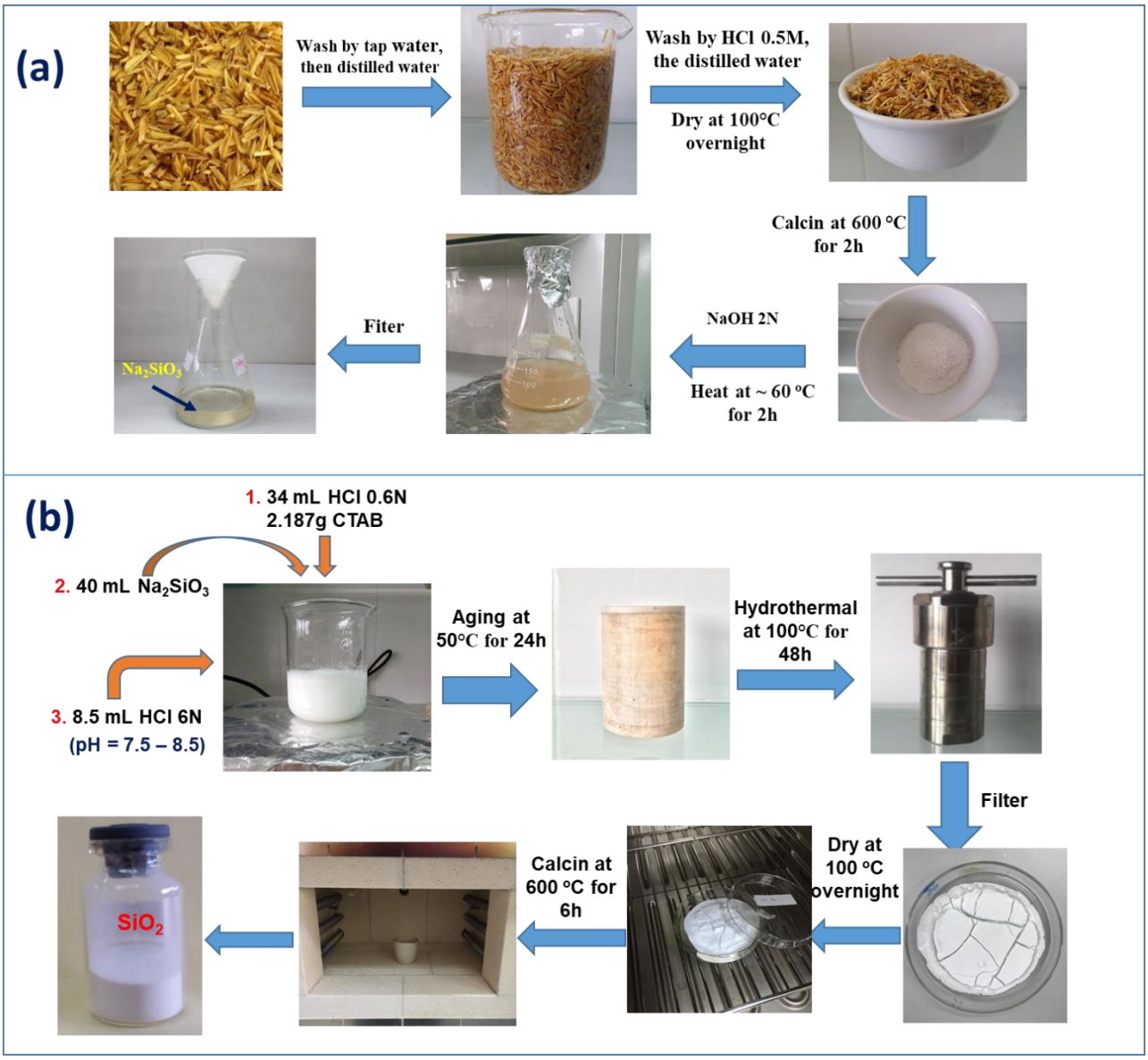

Figure 1. Preparation procedure for porous silica from rice husk.

JEOL-7600F) and a transmission electron microscopy (TEM, JEM-JEOL 2100). The crystalline phase of materials was investigated by X-ray power diffraction (XRD: Bruker D8 Ax XRD-diffractometer). The XRD patterns were obtained with Cu K_α irradiation (40 kV, 40 mA) at the 2θ ranging from 10 to 80°. The textural properties of the samples were measured via N_2 adsorption/desorption isotherms using a Micromeritics (Gemini VII 2390). The specific surface area, pore volume, and pore diameter of the as-synthesized materials were obtained by using the Brunauer-Emmett-Teller (BET) method. The Fourier transform infrared spectroscopy (FT-IR) was measured by Madison, WI, USA measurement to explore the changes in functional groups of the ZnO•SiO_2 nanocomposite by Nicolet IS50.

2.5 Photocatalytic Test

The ability of the as-synthesized materials to degrade organic substances was investigated in a batch test. Typically, 50 mg of the composite was added to a 250 mL glass beaker containing 100 mL of the organic substance 10 mg/L. At specific time intervals of 10 min, 2 mL of the suspension sample was withdrawn and then filtered by a syringe filter (0.45 μm PTFE membrane) to remove the material. The concentration of organic substance in the filtrate was analyzed by a UV-Vis spectrophotometer (Agilent 8453). The organic substance degradation efficiency (D_e) was calculated by Equation (1) [13,15,16]:

$$D_e\ (\%) = \frac{C_0 - C_t}{C_0} \times 100\% \quad (1)$$

The organic substance photodegradation rate can be evaluated by using the pseudo-first-order model as Equation (2) [13,15,16]:

$$\ln\left(\frac{C_0}{C_t}\right) = kt \quad (2)$$

where, C_0 and C_t are the organic substance concentration at initial (t = 0) and time t (min), respectively. k is the pseudo first-order rate constant. The k value was calculated from the slope of the ln (C_0/C_t) – t plots.

To compare the degradation organic substance of the ZnO•SiO_2 nanocomposite, a series of organic matter degradation experiments including tartrazine (TA), congo red (CR), methyl blue (MB), caffeine, and tetracycline hydrochloride (TCH), performed similar to the JGB degradation process. The conditions of each reaction are detailed in Table 2.

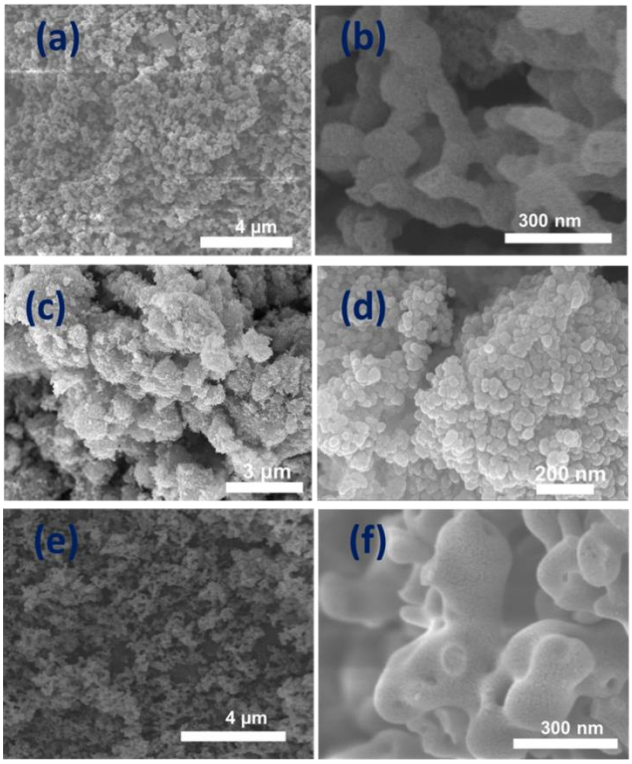

Figure 2. FE-SEM images of (a-b) porous SiO_2, (c-d) ZnO nanoparticle, and (e-f) ZnO•SiO_2 nanocomposite.

3. Results and Discussion

3.1. Characterization of the As-synthesized Materials

3.1.1 SEM analysis

The morphology of as-synthesized materials was observed by SEM method and that is presented in Figure 2. The porous SiO_2 was in the amorphous form and had a ragged surface, which was attributed to the nanopores as shown in Figure 2(a-b). The pore diameter was about 10.0 nm, confirmed by N_2 adsorption and desorption analysis (Table 1). These nanopores greatly increase the specific surface area of amorphous SiO_2 and add to their adsorption ability. The

Table 1. Textural properties of the SiO_2 and ZnO•SiO_2 samples.

Samples	S_{BET} (m^2/g)	BJH Pore volume (cm^3/g)	Average pore width (nm)
SiO_2	496.9	1.44	10.0
ZnO	26.4	0.48	53.7
ZnO•SiO_2	34.1	0.57	57.8

unique microporous structure and environmentally friendly characteristics make SiO_2 an excellent candidate for a carrier. ZnO nanoparticles aggregate into clusters as shown in Figure 2(c). The hydrothermal method was used to load the ZnO nanoparticles on the porous SiO_2 material. Initially, the zinc acetate solution entered the pores, and then, the ZnO was deposited as the reactions of that solution with HMTA and NH_4OH had finished. Figure 2(e-f) shows the SEM images of the ZnO•SiO_2 nanocomposite. It could be observed that ZnO with rod-like shape growth on the surface of SiO_2, the growth directions of the nanorods appeared relatively random on nonplanar substrates. The bulk shape had an average length of about 1.5 µm and a width of about 200 nm.

3.1.2 TEM analysis

Figure 3 shows the TEM image of the as-synthesized materials. The porous SiO_2 has an amorphous morphology with a dense pore system as shown in Figure 3(a-b). The pore diameters were about 10.0 nm, this result was suitable with the SEM and N_2 adsorption/desorption results. Similar to the results of SEM analysis, TEM images of the ZnO material (Figure 3(c-d)) also show that ZnO nanoparticles with a size of about 20 - 35 nm agglomerate into clusters and overlap each other. The ZnO nanoparticles were pretty even. As shown in Figure 3(e-h), it can be observed that the ZnO nanoparticles growth on the surface of the porous SiO_2 material, which filled the pores of the SiO_2 material. The combination of crystalline ZnO nanoparticles and amorphous SiO_2 materials can be seen in Figure 3(g). The ZnO nanoparticles exhibited the (101) crystal plane of the hexagonal wurtzite structure, with the distance between the aircraft being 0.25 nm (Figure 3(h)). Thus, the ZnO nanoparticles were loaded on the pores and surface of SiO_2 materials by the hydrothermal method.

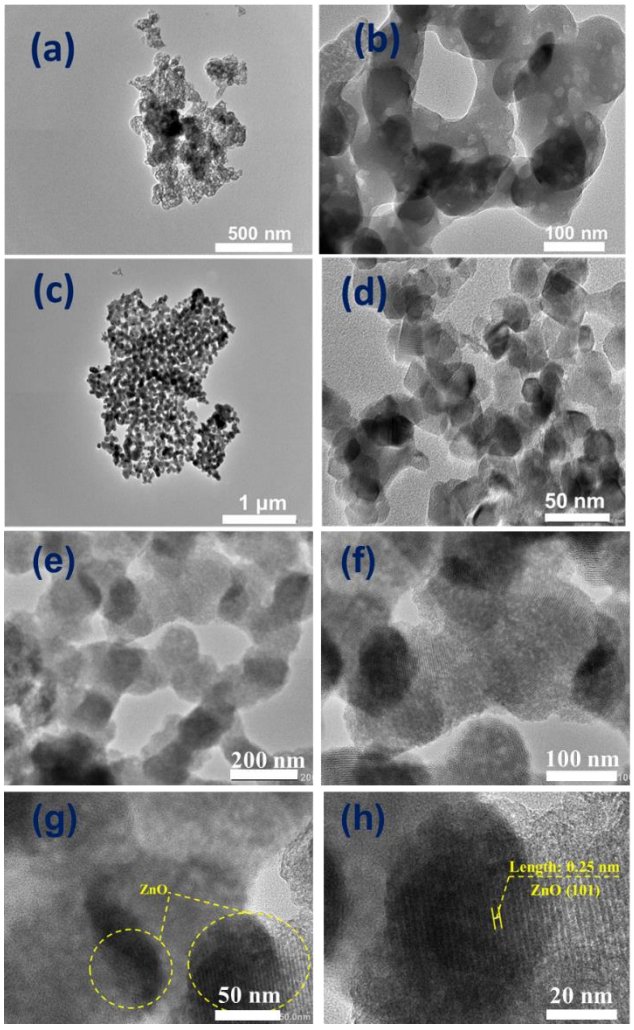

Figure 3. TEM images of (a-b) porous SiO_2, (c-d) ZnO nanoparticles, and (e-h) ZnO•SiO_2 nanocomposite.

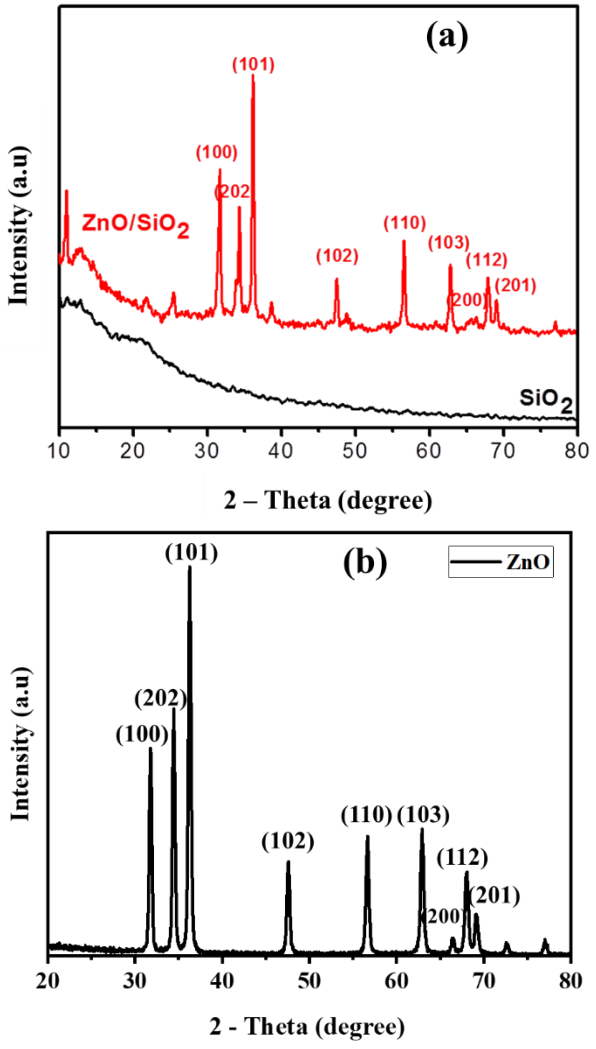

Figure 4. XRD patterns of the porous (a) SiO_2, ZnO•SiO_2, and (b) ZnO samples.

3.1.3 XRD analysis

Figure 4 shows the XRD patterns of the porous SiO_2 carrier, ZnO nanoparticle, and $ZnO•SiO_2$ nanocomposite. The XRD pattern of the porous SiO_2 material shows two strong peaks at 14° and 23°, indicating that the main phase was an amorphous phase corresponding to amorphous SiO_2. In the XRD pattern of the $ZnO•SiO_2$ nanocomposite, in addition to the amorphous peaks of the porous SiO_2 materials, the main peaks of the ZnO nanoparticles were identified at 2θ = 32.5°, 34.9°, 37.1°, 47.60°, 56.65°, 62.92°, 66.05°, 67.99°, 69.19° were identified, corresponding to the (100), (202), (101), (102), (110), (103), (200), (112), and (201) planes [17-19]. These peaks can be assigned to the hexagonal wurtzite structure of ZnO (JCPDS 36-1451) [20]. Thus, the ZnO nanoparticles with hexagonal wurtzite structure were successfully loaded into the porous SiO_2.

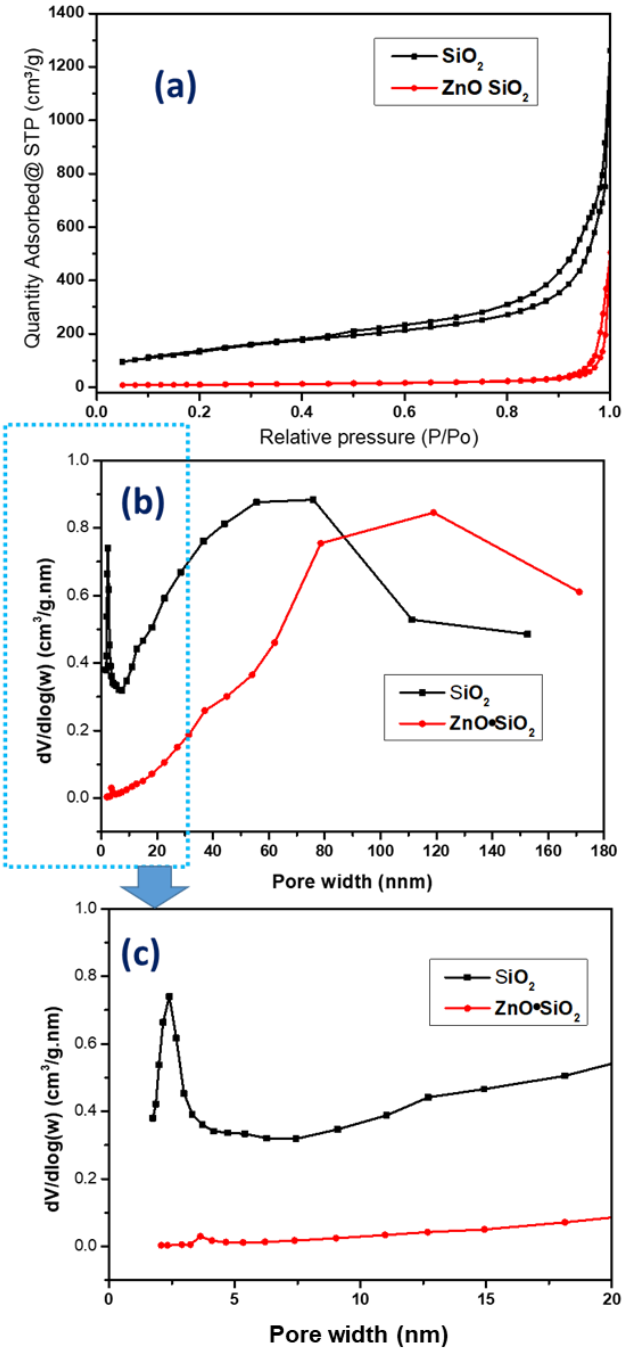

Figure 5. (a) N_2 adsorption/desorption isotherms, (b) and (c) pore size distributions of the porous SiO_2 and $ZnO•SiO_2$ samples.

3.1.3 N_2 adsorption/desorption isotherm

The N_2 adsorption/desorption isotherms and the pore size distributions of the porous SiO_2 and $ZnO•SiO_2$ nanocomposite are shown in Figure 5. It can be seen that the N_2 adsorption capacity and pore volume (1.44 cm^3/g) of SiO_2 were significantly higher than those of the $ZnO•SiO_2$ nanocomposite (pore volume 0.57 cm^3/g), indicating that the ZnO nanoparticles were loaded into the porous SiO_2 and occupied a certain amount of pore volume, resulting in a decrease in the nitrogen adsorption. Table 1 summarizes three physical parameters, namely the surface area, total pore volume, and average pore diameter of the amorphous SiO_2 and $ZnO•SiO_2$ materials. These data show that the porous SiO_2 material had the large surface area and pore volume, confirming its stronger adsorption ability and great potential for application as a carrier. After loading with the ZnO nanoparticles, these parameters of the porous SiO_2 were significantly reduced due to the ZnO nanoparticles filled the pores and blocked the absorption of N_2. These indicates that the ZnO nanoparticles were successfully loaded into the micropores of the amorphous SiO_2 material.

3.1.4 FT-IR analysis

The FT-IR was used to analyze the chemical groups of the as-synthesized materials and also to assess whether a chemical reaction took place between the ZnO nanoparticles and the amorphous SiO_2 materials. As shown in Figure 6,

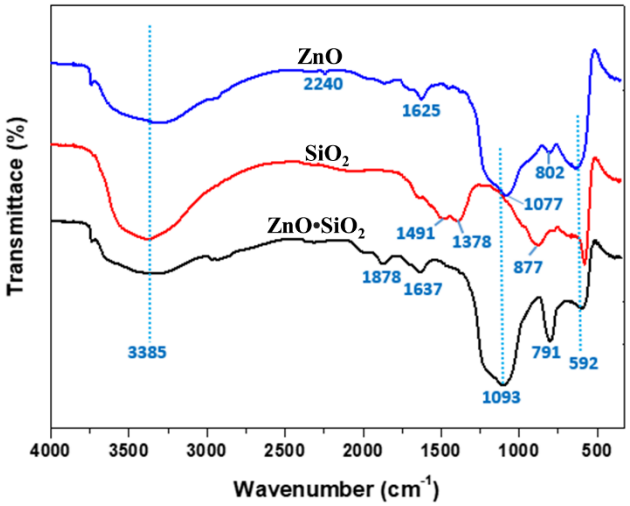

Figure 6. FT-IR spectra of the porous SiO_2, ZnO, and $ZnO•SiO_2$ materials.

the carbonyl stretching vibration peak ($\upsilon_{C=O}$ 1529 cm^{-1}) of the ZnO did not migrate after loading into the SiO_2 materials. This shows that there were no hydrogen bonds between ZnO and SiO_2. Moreover, the carbonyl stretching vibration peak of the ZnO nanoparticles became weaker after loading into the amorphous SiO_2 materials, which may be due to the embedding effect of the SiO_2 materials. Compared with the infrared spectra of ZnO and SiO_2, there were no new peak formations in the spectra of the ZnO•SiO_2 nanocomposite, indicating that the ZnO and SiO_2 did not chemically react but formed physical adsorption.

3.2 Comparison of the Degradation Organic Substance of the ZnO•SiO_2 Nanocomposite

A series of experiments were carried out on the organic degradation of the ZnO•SiO_2 nanocomposite. The reaction conditions and study results are present in Table 2. It can be seen that the ZnO•SiO_2 nanocomposite can degrade most of the dyes in an aqueous environment. Especially, 99.98% CR was degraded within 5 min. As shown in Table 2, the ZnO•SiO_2 nanocomposite degraded not only the dyes, but also other organic substances such as caffeine (89.97%) and tetracycline hydrochloride (98.97%). These results show that ZnO nanoparticles doped on SiO_2 effectively promotes their catalytic ability. The tiny size, high pore volume (0.57 cm^3/g), and large surface area (34.1 m^2/g) can enhance the interaction between the ZnO•SiO_2 nanocomposite and the organic pollutants. This improves the ability to degrade these pollutants. It can be concluded that the ZnO•SiO_2 nanocomposite has an excellent ability to degrade organic substances.

Several studies of the JGB degradation are listed in Table 3 to compare the degradation ability of the different materials. A variety of materials have been investigated including

Table 2. The degradation organic substances of the ZnO•SiO_2 nanocomposite.

Organic substance	Reaction conditions	Observation
Janus Green B (JGB)	[ZnO•SiO_2] = 0.5 g/L, [JGB] = 10 mg/L, and under a 250 W Hg lamp	97.87 % JGB was degraded after 60 min
Tartrazine (TA)	[ZnO•SiO_2] = 0.5 g/L, [TA] = 10 mg/L, and under a 250 W Hg lamp	99.37 % TA was degraded after 30 min
Congo Red (CR)	[ZnO•SiO_2] = 0.5 g/L, [CR] = 10 mg/L, and under a 250 W Hg lamp	99.98 % CR was degraded after 5 min
Methyl Blue (MB)	[ZnO•SiO_2] = 0.5 g/L, [MB] = 10 mg/L, and under a 250 W Hg lamp	99.84 % MB was degraded after 50 min
Caffeine	[ZnO•SiO_2] = 0.5 g/L, [Caffeine] = 10 mg/L, and under a 250 W Hg lamp	89.97 % Caffeine was degraded after 60 min
Tetracycline Hydrochloride (TCH)	[ZnO•SiO_2] = 0.5 g/L, [TCH] = 10 mg/L, and under a 250 W Hg lamp	98.97 % TCH was degraded after 60 min

Table 3. Some study results on the JGB degradation.

Catalyst	Reaction conditions	Observation	Reference
ZnO•SiO_2	[ZnO•SiO_2] = 0.5 g/L, [JGB] = 10 mg/L, pH = 6, and under a 250 W Hg lamp	97.87 % JGB was degraded after 60 min	This study
Au/ZnO	[Au/ZnO] = 0.5 g/L, [JGB] = 10 mg/L, pH = 6, and under a 250 W Hg lamp	98.97 % JGB was degraded after 100 min	[21]
TiO_2	[TiO_2] = 2.0 g/L, [JGB] = 0.2 g/L, and under a 300 W tungsten visible lamps	76 % JGB was degraded after 90 min	[22]
Sr-TiO_2	[Sr-TiO_2] = 2.0 g/L, [JGB] = 0.2 g/L, and under a 300 W tungsten visible lamps	92 % JGB was degraded after 90 min	[22]
Ag•ZnO•Activated Carbon (Ag•ZnO•AC)	[Ag•ZnO•AC] = 0.5 g/L, [JGB] = 10 mg/L, pH = 6.5, and under a 250 W Hg lamp	100 % JGB was degraded after 60 min	[23]

Au/ZnO [21], TiO_2 [22], Sr-TiO_2 [22], and Ag•ZnO•Activated Carbon (Ag•ZnO•AC) [23]. Each study has different reaction conditions. Therefore, it is very difficult to compare objectively. As shown in Table 3, the JGB degradation efficiency of the ZnO•SiO_2 nanocomposite was lower than that of other materials. However, the ZnO•SiO_2 nanocomposite has JGB degradation ability in a short time and achieved the degradation efficiency of 97.87 %. Besides, unlike the Au/ZnO or Ag•ZnO•AC materials, the ZnO•SiO_2 nanocomposite was synthesized from RH, which is cheap and environmentally friendly. Thus, the ZnO•SiO_2 nanocomposite is both only time-saving and cost saving and above all environmentally friendly.

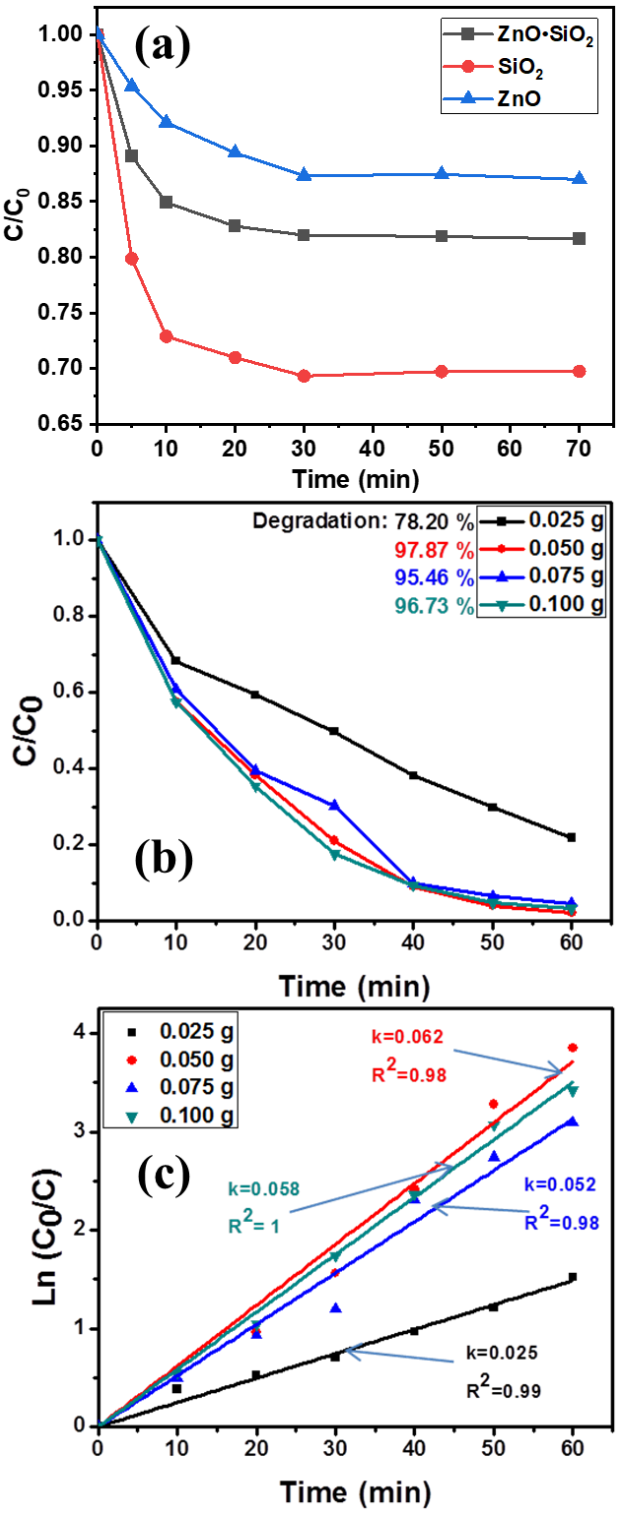

Figure 7. (a) The JGB adsorption capacity of the as-synthesized materials, (b) effect of the ZnO•SiO_2 composite dosage on the JGB degradation process and (c) the first-order kinetic curves. Reaction conditions: [JGB] = 10 mg/L, [ZnO•SiO_2] = 0.25–1.00 g/L, pH = 6, T = 25 °C, and a 250 W Hg lamp.

3.3 Effect of Reaction Parameters to the JGB Degradation Efficiency

3.3.1 Effect of the ZnO•SiO_2 nanocomposite dosage

The JGB adsorption capacity of the as-synthesized materials was studied and that is shown in Figure 7(a). It can be seen that the as-synthesized materials can adsorb the JGB. The longer the adsorption time, the higher the adsorption capacity of JGB. However, after 30 minutes, adsorption equilibrium was established. Especially, the porous SiO_2 has the best JGB adsorption ability with an efficiency of 30.24%. The JGB adsorption ability of the ZnO nanoparticles was insignificant, which only achieved 12.57% after 70 min. After doping the ZnO nanoparticles into the porous SiO_2, the JGB adsorption efficiency achieved 18.13%. These experimental results are completely consistent with the study of the characteristics of the as-synthesized materials. The higher the pore volume and S_{BET} of the material, the better its adsorption capacity.

To investigate the influence of the ZnO•SiO_2 nanocomposite dosage, the photocatalytic experiments were carried out by employing different amounts of the ZnO•SiO_2 nanocomposite (25, 50, 75, and 100 mg) under the constant conditions: [JGB] = 10 mg/L, reaction temperature of 25 °C, and pH = 6. The JGB degradation efficiency and reaction rate at the different ZnO•SiO_2 nanocomposite dosages are shown in Figure 7(b-c). For the ZnO•SiO_2 nanocomposite dosage of 0.25 g/L, the JGB degradation efficiency achieved 78.20 % with the reaction rate of 0.025 min^{-1}. When the ZnO•SiO_2 nanocomposite dosage was increased to 0.5 g/L, the JGB degradation efficiency and reaction rate were also significantly increased. It can be seen that there was an appreciable increase in the reaction rate of JGB degradation with increasing the ZnO•SiO_2 nanocomposite dosage. The reason for this observation is thought to be that increasing photocatalyst dosage results in an increase in the number of active sites available at the surface of

the catalyst [24]. Another acceptable explanation is that the density of catalyst particles in the illumination area is improved after the ZnO•SiO_2 nanocomposite dosage was increased [25,26]. However, when surpassing the limit value because the suspension is increased, the short wave tail photons cannot enter the reaction mixture and the decrease in UV light penetration as a result of increased scattering effect [27], the degradation efficiency decreased. As the JGB degradation efficiency at the ZnO•SiO_2 nanocomposite dosage of 1.0 g/L was 96.73% with the reaction rate of 0.058 min^{-1}. Thus, with the JGB degradation efficiency of 97.87% and reaction rate of 0.062 min^{-1}, the ZnO•SiO_2 nanocomposite dosage of 0.5 g/L was chosen as the optimal dosage for the smooth JGB degradation process.

3.3.2 Effect of initial JGB concentration

Figure 8 shows the effect of the initial JGB concentration on the JGB degradation efficiency. Experiments were conducted by varying the initial JGB concentration from 5 to 20 mg/L. The ZnO•SiO_2 nanocomposite dosage, reaction temperature, and initial pH were constant at 0.5 g/L, 25 °C, and 6, respectively. It can be seen that the initial JGB degradation efficiency was significantly lowered with an increase in the initial JGB concentration. The JGB degradation efficiency with the initial JGB concentration of 5 mg/L increased sharply in the initial 60 min (100.0%). In contrast, for the more highly JGB concentrations, such as the initial JGB concentration of 20 mg/L, only 59.94% JGB loss was observed after the same reaction time. It can be seen that the higher the initial JGB concentration, the longer the reaction time and the decrease in the JGB degradation efficiency.

This effect can be interpreted by the following reasons: When the increases of the initial JGB concentration, the photons get intercepted before they can reach the surface of the ZnO•SiO_2 nanocomposite, resulting in the generation of •OH and $•O_2^-$ radical decreases, meaning the

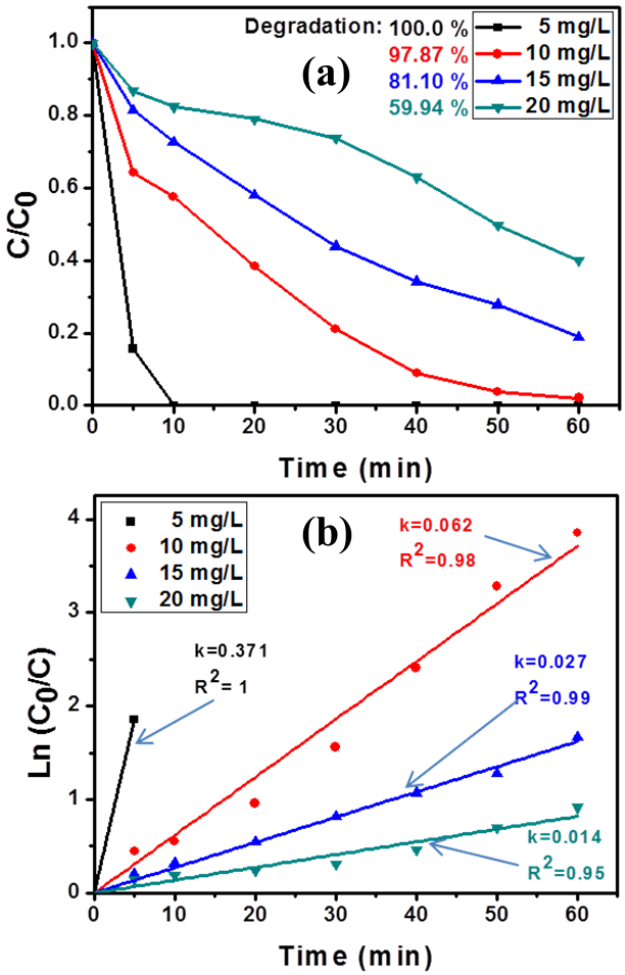

Figure 8. (a) Effect of the initial dye concentration on the JGB degradation process and (b) the first-order kinetic curves. Reaction conditions: [JGB] = 5–20 mg/L, [ZnO•SiO_2] = 0.5 g/L, pH = 6, and T = 25 °C, and a 250 W Hg lamp.

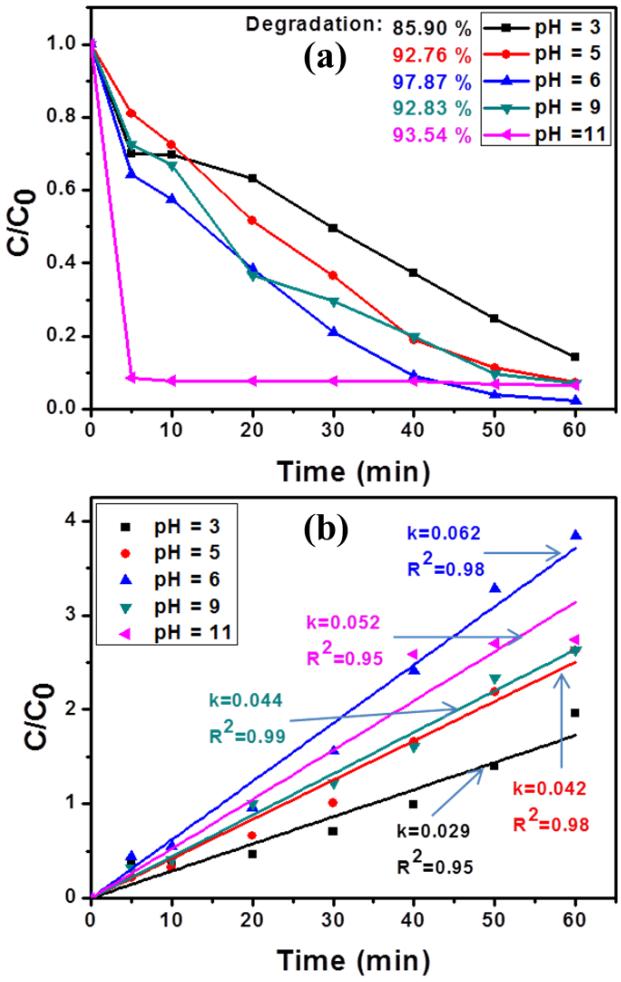

Figure 9. (a) Effect of the initial pH on the JGB degradation process and (b) the first-order kinetic curves. Reaction conditions: [JGB] = 10 mg/L, [ZnO•SiO_2] = 0.5 g/L, pH = 3-11, and T = 25 °C, and a 250 W Hg lamp.

JGB degradation efficiency decreases and a large number of the JGB molecules along with the intermediates generated may compete for the constant total active sites available for adsorption at the fixed ZnO•SiO_2 nanocomposite dosage [25,28]. Additionally, with the increase in the initial JGB concentration, the solution becomes more intensely colored and the path length of photons entering into the solution decreases [29], thus the absorption of photons by the ZnO•SiO_2 nanocomposite decreases, and consequently the degradation rate is reduced.

3.3.3 Effect of initial pH

The pH solution is an important parameter in photocatalytic degradation reactions for industrial applications [30,31], thus the effect of initial pH solution to remove dye was examined and the result is presented in Figure 9. The effect of initial pH solution on degradation of JGB was investigated in the pH range of 3–11, at the ZnO•SiO_2 nanocomposite dosage of 0.5 g/L, the initial JGB concentration of 10 mg/L, and reaction temperature of 25 °C. The pH of the JGB solution was adjusted by NaOH 0.1 M and HCl 0.1 M, before light irradiation and it was not controlled during the reaction. The obtained results indicated that the JGB degradation process was significantly influenced by the initial pH. In the initial 5 min, the JGB degradation rate and degradation efficiency increased significantly when the initial pH increased from 3 to 11. The JGB degradation efficiency for the initial pH of 3, 5, 6, 9, and 11 were 85.90%, 92.76%, 97.87%, 92.83%, and 93.54%, respectively, in the reaction time of 60 min. It can be seen that the alkaline condition was very beneficial to the JGB degradation process. The initial pH solution of 6 was chosen as the optimal condition because the JGB degradation efficiency and rate were the highest at 97.85% and 0.062 min^{-1}, respectively.

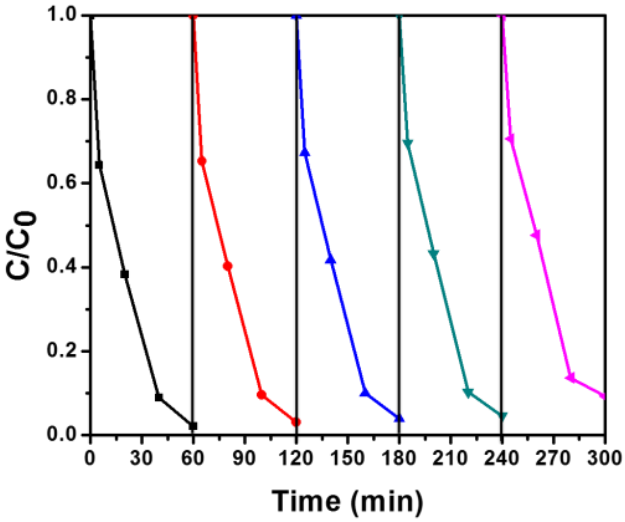

Figure 10. Reusability test of the ZnO•SiO_2 nanocomposite.

3.4 Reusable of the ZnO•SiO_2 Nanocomposite

One of the major advantages of the ZnO•SiO_2 nanocomposite was the reusability. Therefore, the stability of catalytic activity of the ZnO•SiO_2

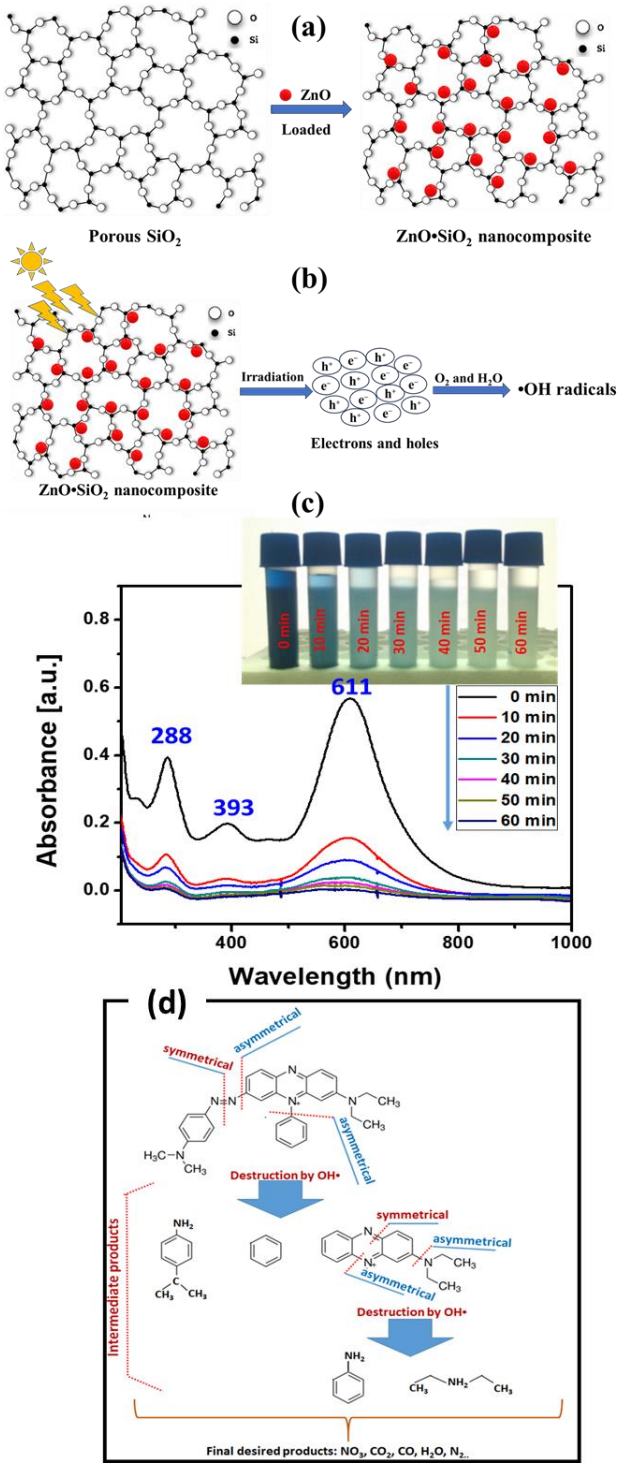

Figure 11. (a) ZnO loaded on SiO_2, (b) generation of free radical, (c) UV-Vis spectral change of the JGB solution during degradation along the reaction time, and (d) possible pathway for the destruction of JGB by ZnO•SiO_2 composite.

nanocomposite is significant for practical application. In this work, repeated tests were conducted to determine the decrease of catalytic activity of the $ZnO•SiO_2$ nanocomposite. As shown in Figure 10, the decolorization ratio in one-hour reaction decreased gradually from 97.87% at the first test to 97.80% at the third test and it kept almost constant at the following two tests. The catalytic activity could be maintained at relatively high level and kept stable. This proves that this $ZnO•SiO_2$ nanocomposite could be a potential product for practical application.

3.5 JGB Degradation Mechanism

The degradation mechanism of JGB was proposed and that is presented in Figure 11. The porous SiO_2 material was synthesized from RH, then the ZnO nanoparticles were loaded into the pores and surface of the SiO_2 material, resulting in the $ZnO•SiO_2$ nanocomposite, as shown in Figure 11(a). When the energy of the irradiated photons is higher than the energy of the band gap of the ZnO nanoparticles, electrons and holes are generated on the $ZnO•SiO_2$ nanocomposite. At the same point, they react with the H_2O in the solution and the O_2 in the air to form the •OH radicals, as shown in Figure 11(b).

The UV-Vis spectral change of JGB and the colour of the dye solution were measured in a time interval of 10 min during degradation, in Figure 11(c). Before oxidation (t = 0), the absorption spectra of JGB was characterized by the bands in the ultraviolet region at 288 and 393 nm and by another band in visible region at 611 nm. The peak at 288 nm is due to the benzene-like structure of the molecules, while the bands in the visible region are associated with the chromophore containing an azo bond [23]. The disappearance of the absorption peak at 611 nm with the reaction time could stem from the fragmentation of the azo links by oxidation [32]. The decrease in intensity of band at 393 nm could be attributed to breaking the −N−C− bond [2]. In addition to this rapid degradation, the decay of the absorbance at 288 nm was considered as the evidence of degradation of aromatic fragments in the dye molecule and its intermediates. Moreover, the different base line in UV-vis spectra was observed, but the maximum absorption had no displacement, it was assigned to formation of intermediate products. According to the UV-vis absorption spectra, the possible route of the destruction of JGB by as-synthesized $ZnO•SiO_2$ composite was suggested in Figure 11(d). Thus, under irradiation of the 250 W Hg lamp, the $ZnO•SiO_2$ nanocomposite made the •OH radicals to destruct the JGB to the environmentally friendly products.

4. Conclusions

In summary, zinc oxide on SiO_2 prepared rice husk was successfully synthesized. The $ZnO•SiO_2$ nanocomposite had a high specific surface area and the activity composite was stable in the degradation reaction. The degradation of JGB dye molecules mainly occurred on the surface of the $ZnO•SiO_2$ nanocomposite. The gradual decrease in the activity of the degradation reaction during the first three tests was attributed to the decrease in the SiO_2 adsorption capacity of the $ZnO•SiO_2$ nanocomposite. This catalyst could still maintain a relatively high and stable activity during the 5 tests. The $ZnO•SiO_2$ nanocomposite not only degraded the dyes but also other organic substances including caffeine and TCH. This nanocomposite is a promising and potential material because of its economical and environmentally friendly material.

Acknowledgements

Thu Huong Nguyen was funded by the Master, PhD Scholarship Programme of Vingroup Innovation Foundation (VINIF), code VINIF.2023.ThS.061.

CRediT Authors Statement

Author Contributions: Thu Huong Nguyen: Methodology, Investigation, Resources, Experiment, and Writing; Tuan Cuong Vu, Trung Phong Le, and Thu Huyen Nguyen: Investigation and Experiment ; Xuan Truong Do and Anh-Tuan Vu: Review, Editing, and Validation. All authors have read and agreed to the published version of the manuscript.

Reference

[1] Food and Agriculture Organization of the United Nations (2024). *GIEWS - Global Information and Early Warning System*. Available: https://www.fao.org/giews/countrybrief/country.jsp?code=VNM

[2] Vu, A.-T., Xuan, T.N., Lee, C.-H. (2019). Preparation of mesoporous Fe_2O_3-SiO_2 composite from rice husk as an efficient heterogeneous Fenton-like catalyst for degradation of organic dyes. *Journal of Water Process Engineering,* 28, 169-180. DOI: 10.1016/j.jwpe.2019.01.019..

[3] Vu, A.-T., Nguyen, T.H., Nguyen, T.H. (2023). Preparation of carnation-like Ag-ZnO composites for enhanced photocatalysis under visible light. *Nanotechnology,* 34(27), 275602. DOI: 10.1088/1361-6528/acca24.

[4] Nguyen, T.H., Nguyen, V.D., Vu, A.-T. (2024). Synthesis of CS-Fe_3O_4/GO nanocomposite for adsorption of heavy metal in aqueous environment. *Nanotechnology,* 35, 345705. DOI: 10.1088/1361-6528/ad50e3.

[5] Vu, A.-T., Nguyen, M.V., Nguyen, T.H. (2024). Fabrication of ethylenediaminetetraacetic modified porous silica composite from rice husk for enhancing the remove of Pb2+ from aqueous solution. *Results in Materials*, 21, 100525. DOI: 10.1016/j.rinma.2023.100525.

[6] Moussavi, G., Mahmoudi, M. (2009). Removal of azo and anthraquinone reactive dyes from industrial wastewaters using MgO nanoparticles. *Journal of Hazardous Materials*, 168(2), 806-812. DOI: 10.1016/j.jhazmat.2009.02.097

[7] Zhu, Q., Wang, W.-S., Lin, L., Gao, G.-Q., Guo, H.-L., Du, H., Xu, A.-W. (2013). Facile Synthesis of the Novel Ag3VO4/AgBr/Ag Plasmonic Photocatalyst with Enhanced Photocatalytic Activity and Stability. *The Journal of Physical Chemistry C,* 117(11), 5894-5900. DOI: 10.1021/jp400842r.

[8] Batool, S., Imran, Z., Hassan, S., Rasool, K., Ahmad, M., Rafiq, M. (2016). Enhanced adsorptive removal of toxic dyes using SiO2 nanofibers. *Solid State Sciences*, 55, 13-20. DOI: 10.1016/j.solidstatesciences.2016.02.001

[9] Thu, H.T., Dat, L.T., Tuan, V.A. (2019). Synthesis of mesoporous SiO_2 from rice husk for removal of organic dyes in aqueous solution. *Vietnam Journal of Chemistry,* 57(2), 175-181. DOI: 10.1002/vjch.201900012.

[10] Aguado, J., Van Grieken, R., López-Muñoz, M.-J., Marugán, J. (2006). A comprehensive study of the synthesis, characterization and activity of TiO_2 and mixed TiO_2/SiO_2 photocatalysts. *Applied Catalysis A: General,* 312, 202-212. DOI: 10.1016/j.apcata.2006.07.003.

[11] Jia, Z.-G., Peng, K.-K., Li, Y.-H., Zhu, R.-S. (2012). Preparation and photocatalytic performance of porous ZnO microrods loaded with Ag. *Transactions of Nonferrous Metals Society of China,* 22(4), 873-878. DOI: 10.1016/S1003-6326(11)61259-4.

[12] Pham, T.A.T., Tran, V.A., Le, V.D., Nguyen, M.V., Truong, D.D., Do, X.T., Vu, A.-T. (2020). Facile preparation of ZnO nanoparticles and Ag/ZnO nanocomposite and their photocatalytic activities under visible light. *International Journal of Photoenergy,* 2020, 8897667. DOI: 10.1155/2020/8897667.

[13] Nguyen, T.H., Cong, T.A.N., Vu, A.-T. (2023). Synthesis of Carnation-Like ZnO for Photocatalytic Degradation of Antibiotics, Including Tetracycline Hydrochloride. *Environmental Engineering Science*, 40(8), 329–339. DOI: 10.1089/ees.2023.0034.

[14] Tu, V.A., Tuan, V.A. (2018). A facile and fast solution chemistry synthesis of porous ZnO nanoparticles for high efficiency photodegradation of tartrazine. *Vietnam Journal of Chemistry,* 56(2), 214-219. DOI: 10.1002/vjch.201800016.

[15] Nguyen, T.H., Vu, A.-T. (2023). Investigation of enhanced degradation of the antibiotic under visible in novel B/ZnO/TiO_2 nanocomposite and its electrical energy consumption. *Nanotechnology,* 35(1), 015709. DOI: 10.1088/1361-6528/acffce.

[16] Tuấn, V.A., Minh, P.Q., Anh, N.T.T., Vi, Đ.T.C., Hằng, N.T.B., Hương. N.T. (2024). Tổng hợp vật liệu Ag/ZnO/g-C_3N_4 bằng phương pháp nung đơn giản để loại bỏ kháng sinh tetracycline hydrochloride trong môi trường nước *Journal of Control Vaccines Biologicals,* 4(1), 142. DOI: 10.56086/jcvb.v4i1.142.

[17] Ahmad, M., Ahmed, E., Hong, Z.L., Ahmed, W., Elhissi, A., Khalid, N.R. (2014). Photocatalytic, sonocatalytic and sonophotocatalytic degradation of Rhodamine B using ZnO/CNTs composites photocatalysts. *Ultrasonics Sonochemistry,* 21(2), 761-773. DOI: 10.1016/j.ultsonch.2013.08.014.

[18] Zuo, Z., Liao, R., Zhao, X., Song, X., Qiao, Z., Guo, C., Zhuang, A., Yuan, Y. (2017). Anti-frosting performance of superhydrophobic surface with ZnO nanorods. *Applied Thermal Engineering,* 110, 39-48. DOI: 10.1016/j.applthermaleng.2016.08.145.

[19] Perillo, P.M., Atia, M.N., Rodríguez, D.F. (2017). Effect of the reaction conditions on the formation of the ZnO nanostructures. *Physica E: Low-dimensional Systems and Nanostructures*, 85, 185-192. DOI: 10.1016/j.physe.2016.08.029.

[20] Nguyen, T.H., Mai, T.T., Tran, T.P., Thi, C.L.T., Thi, C.V.D., Thi, M.L.V., Nguyen, M.V., Nguyen, T.H., Vu, A.-T. (2024). Studying the Nanocomposite B/ZnO for Photocatalysis: Facile Control the Morphology via Sol-gel Method and Antibiotic Degradation Investigations. *Journal of Sol-Gel Science and Technology*, 110, 319–332. DOI: 10.1007/s10971-024-06359-z.

[21] Vu, A.-T., Pham, T.A.T., Do, X.T., Tran, V.A., Le, V.D., Truong, D.D., Nguyen, T.H., Nguyen, M.V. (2021). Preparation of hierarchical structure au/ZnO composite for enhanced photocatalytic performance: characterization, effects of reaction parameters, and oxidizing agent investigations. *Adsorption Science and Technology*, 2021, 5201497. DOI: 10.1155/2021/5201497.

[22] Keerthana, S., Yuvakkumar, R., Ravi, G., Thambidurai, M., Nguyen, H.D., Velauthapillai, D. (2023). Sr doped TiO2 photocatalyst for the removal of Janus Green B dye under visible light. *RSC Advances*, 13(27), 18779-18787. DOI: 10.1039/D3RA00567D.

[23] Vu, A.-T., Pham, T.A.T., Tran, T.T., Nguyen, X.T., Tran, T.Q., Tran, Q.T., Nguyen, T.N., Doan, T.V., Vi, T.D., Nguyen, C.L. (2020). Synthesis of nano-flakes Ag• ZnO• activated carbon composite from rice husk as a photocatalyst under solar light. *Bulletin of Chemical Reaction Engineering & Catalysis*, 15(1), 264-279. DOI: 10.9767/bcrec.15.1.5892.264-279.

[24] Subash, B., Krishnakumar, B., Swaminathan, M., Shanthi, M. (2013). Highly Efficient, Solar Active, and Reusable Photocatalyst: Zr-Loaded Ag–ZnO for Reactive Red 120 Dye Degradation with Synergistic Effect and Dye-Sensitized Mechanism. *Langmuir*, 29(3), 939-949. DOI: 10.1021/la303842c.

[25] Akyol, A., Yatmaz, H.C., Bayramoglu, M. (2004). Photocatalytic decolorization of Remazol Red RR in aqueous ZnO suspensions. *Applied Catalysis B: Environmental*, 54(1), 19-24. DOI: 10.1016/j.apcatb.2004.05.021.

[26] Krishnakumar, B., Swaminathan, M. (2012). Photodegradation of Acid Violet 7 with AgBr–ZnO under highly alkaline conditions. *Spectrochimica Acta Part A: Molecular and Biomolecular Spectroscopy*, 99, 160-165. DOI: 10.1016/j.saa.2012.08.077.

[27] Lang, X., Chen, X., Zhao, J. (2014). Heterogeneous visible light photocatalysis for selective organic transformations. *Chemical Society Reviews*, 43, 473-486. DOI: 10.1039/C3CS60188A.

[28] Behnajady, M.A., Modirshahla, N., Hamzavi, R. (2006). Kinetic study on photocatalytic degradation of C.I. Acid Yellow 23 by ZnO photocatalyst. *Journal of Hazardous Materials*, 133(1), 226-232. DOI: 10.1016/j.jhazmat.2005.10.022.

[29] Krishnakumar, D.B., Swaminathan, M. (2013). Solar photocatalytic degradation of Naphthol Blue Black. *Desalination and Water Treatment*, 51, 34-36. DOI: 10.1080/19443994.2013.792131.

[30] Nguyen, T.H., Vu, A.-T. (2022). Preparation of B/ZnO Nanocomposite by Simple Mechanical Combustion Method for Removal of Antibiotics in Aqueous Environments. *Bulletin of Chemical Reaction Engineering & Catalysis*, 17(4), 786-797. DOI: 10.9767/bcrec.17.4.16090.786-797.

[31] Tuan, V.A., Huong, N.T., Viet, N.M. (2024). Novel B/ZnO material for enhanced degradation of tetracycline hydrochloride in an aqueous environment under visible light. *Journal of Science & Technology*, 60(3), 43-50. DOI: 10.57001/huih5804.2024.096.

[32] Zhang, Y.Z.H., Zhang, D.B. (2007). Decolorization and mineralization of CI Reactive Black 8 by Fenton and ultrasound/Fenton method. *Coloration Technology*, 123, 101-105. DOI: 10.1111/j.1478-4408.2007.00069.x